Journal of Molecular Catalysis A: Chemical 417 (2016) 126–134

Contents lists available at ScienceDirect

Journal of Molecular Catalysis A: Chemical

journal homepage: www.elsevier.com/locate/molcata

Catalytic decarboxylation of non-edible oils over three-dimensional, mesoporous silica-supported Pd

Ravindra Raut, Vikram V. Banakar, Srinivas Darbha *

Catalysis and Inorganic Chemistry Division, CSIR-National Chemical Laboratory, Pune 411 008, India

ARTICLE INFO

Article history:
Received 11 February 2016
Received in revised form 8 March 2016
Accepted 9 March 2016
Available online 11 March 2016

Keywords:
Biofuel
Vegetable oil
Deoxygenation
Mesoporous silica
Supported palladium
Diesel-range hydrocarbons

ABSTRACT

Deoxygenation of fatty acids (oleic and stearic acids) and non-edible oil (jatropha oil) over Pd(1–5 wt%) supported on two structurally different, three-dimensional, mesoporous silica (SBA-12 and SBA-16) catalysts was investigated. Pd/SBA-16 (cubic mesoporous structure with space group $Im\bar{3}m$) showed higher catalytic activity than Pd/SBA-12 (hexagonal mesoporous structure with space group $p6_3/mmc$). The influence of reaction parameters like temperature, H_2 pressure and Pd content as well as the nature of the feedstock on catalytic activity and product selectivity was studied. A temperature of above 320 °C, reaction time of 5 h and Pd content (on silica surface) of 3 wt% enabled complete conversion of the fatty compounds into diesel-range hydrocarbons. Deoxygenation proceeded through hydrodeoxygenation and decarboxylation mechanisms when a saturated (stearic) acid was used as a feed while it advanced mainly through decarboxylation route when an unsaturated (oleic) acid was employed. Higher surface hydrophobicity and smaller size particles of Pd are the possible causes for the superior catalytic activity of Pd/SBA-16.

1. Introduction

According to the world energy council, about 82% of the energy is currently derived from fossil resources (petroleum, natural gas and coal). Usage of fossil fuels has been realized to cause adverse effects to the environment [1,2]. Moreover, at the projected rate of consumption, the availability of petroleum and natural gas is expected to run out in about 70 years and coal in 200 more years. Biofuels show the way to sustainable environment, energy independence, employment to rural population and savings in oil import bill. Vegetable oils such as soybean, rapeseed and palm oils comprise triglycerides (TGs) which can be converted into diesel-like fuels [3–5]. Use of non-edible oils instead of edible ones makes the biofuels production more attractive as the former are cheaper and do not lead to issues like food versus fuel controversy. Non-edible oils contain a significant amount of free fatty acids (FAs) in their composition along with glycerides. One option exists in the form of hydroprocessing for removal of oxygen from the constituent TGs and FAs toward producing diesel-range hydrocarbons (HCs) [6–8]. Fatty acid methyl esters (FAMEs) represent the first generation biodiesel formed via methanolysis of vegetable oils. Unfortunately, use of FAMEs can cause problems in vehicles due to their high oxygen content and viscosity rendering them a less than an ideal fuel for conventional engines. For example, the unburnt part of biodiesel, when mixed with the lubricating oil, can promote engine aging [9]. Further, FAMEs are associated with issues related to cold-flow and oxidation stability. The diesel-like HCs consisting of 15–18 carbon atoms (produced by the hydroprocessing route) provide good fuel properties [10]. Unlike FAMEs, the HC-based biofuels have the advantage of using them as they are or as a blend with the conventional diesel in any proportion.

Two types of catalyst systems were reported for deoxygenation of vegetable oils: (i) Mo and W promoted hydrotreating catalysts (Ni-Mo/Al_2O_3, Ni-W/Al_2O_3, Co-Mo/Al_2O_3 and Co-W/Al_2O_3) [9,11–14] and (ii) supported noble metal catalysts [15–18]. While the mode of deoxygenation is mainly through dehydration (H_2O removal) over the former type catalysts, it is through decarbonylation/decarboxylation (CO/CO_2 removal) on the latter type catalysts. Relatively lesser amount of hydrogen is needed while using the noble metal catalysts (5–20 bar) as against Ni-Mo/W catalysts (50–70 bar). After screening several supported metal catalysts, Snåre et al. [19] found that carbon-supported Pd converts stearic acid completely with >98% selectivity toward heptadecane (C_{17}). The efficiency of deoxygenation of different metals decreased in the order: Pd > Pt > Ni > Rh > Ir > Ru > Os. They found that decarboxylation was profound over Pd/C, while decarbonylation was prevalent

* Corresponding author.
E-mail address: d.srinivas@ncl.res.in (S. Darbha).

http://dx.doi.org/10.1016/j.molcata.2016.03.023
1381-1169/

over a Pt/C catalyst. Alkaline Pd/C led to highest initial rates and conversion, but formed a large quantity of aromatics which was a drawback [20]. Catalytic activity of mesoporous Pd/C in a continuous flow reactor was studied [21]. Conversion of stearic acid declined during a 92 h time-on-stream investigation which was attributed for coking of the catalyst surface. Noble metals supported on zeolites and mesoporous silica were also investigated as catalysts for this reaction. Pt-Re/H-ZSM-5 enabled conversion of jatropha oil (to C_{15}–C_{18} HCs) in yields of 67% at standard hydrotreating conditions [22]. Ahmadi et al. [23] reported oleic acid decarboxylation over Pt supported on small pore zeolites (SAPO-34, DNL-6 and RHO) and hydrotalcites yielding paraffinic, branched and aromatic HCs. They found that catalyst acidity, Pt dispersion and pore diameter of the support influence the product selectivity. Ping et al. [24] studied meso-cellular foam silica (MCF)-supported Pd catalyst in hydrogen-free decarboxylation of FAs. The catalyst showed deactivation. Organic deposition on the catalyst was reported as the cause for its deactivation. Lestari et al. [25] and Lee and Ramli [26] investigated the use of Pd/SBA-15 for converting stearic acid and methyl oleate into HCs. Pd supported on SBA-15 having necklace-like morphology and high surface area exhibited high catalytic activity.

We report here, for the first time, the application of three-dimensional, mesoporous silica (SBA-12 and SBA-16)-supported Pd as catalysts for deoxygenation of FAs (unsaturated oleic acid—OA and saturated stearic acid—SA, as representative examples of FAs) and non-edible jatropha oil. Three-dimensional mesoporosity enables enhanced rate of transport of reactant and product molecules and accessibility of active sites. SBA-12 and SBA-16 differ in their structure, acidity and surface properties which could lend differences in the behavior of the supported Pd. The present study probes these effects on the catalytic deoxygenation activity.

2. Experimental

2.1. Catalyst preparation

Brij-76 [$C_{18}H_{37}(OCH_2CH_2)_{10}OH$, average mol. wt. ~711, Aldrich Co.] and Pluronic F127 block-copolymer ($EO_{106}PO_{70}EO_{106}$, average mol. wt. ~12600, Aldrich Co.) were used as structure directing agents in the synthesis of SBA-12 and SBA-16, respectively. Tetraethylorthosilicate (TEOS, 98%, Aldrich Co.) was used as a Si source. Tetraamminepalladium(II) nitrate (10 wt% in H_2O solution, Aldrich Co.) was used as a Pd source. All the solvents (A.R. grade) were procured from Thomas Baker and the reagents were purchased from Aldrich Co.

SBA-12 was prepared by a modified procedure of Zhao et al. [27], wherein, 8 g of Brij-76 was added to a solution of 40 g of distilled water and 160 g of 0.1 M HCl taken in a polypropylene beaker. It was heated to 40 °C and stirred for 2 h till a homogeneous solution was obtained. To it, 17.6 g of TEOS was added over 30 min. Stirring was continued for another 20 h. The gel formed was transferred into a Teflon-lined stainless steel autoclave (80 ml) and heated at 100 °C for 24 h while placing in an electric oven. The solid (as-synthesized SBA-12) formed was filtered, washed thoroughly with distilled water (2–3 l) and dried at 100 °C for 12 h. It was calcined at 550 °C (heating rate = 4 °C/min) for 8 h to remove all the organic matter in it. The calcined SBA-12 was white in color. Yield: 94%. Palladium was deposited on it by wet impregnation method. In a typical procedure, the calcined SBA-12 (2 g) was suspended in distilled water (15 ml) taken in a glass round-bottom flask. A known quantity of the palladium source (0.5611 g for 1 wt% Pd loading, for example) dissolved in 5 ml of water was added drop-wise to the above suspension. It was stirred over a rotary evaporator at 60 °C for 3 h. Then, water was evaporated by applying vacuum. The gray colored solid formed was collected, calcined at 400 °C (heating rate = 4 °C/min) for 2 h. Just prior to reactions and characterization studies, Pd/SBA-12, thus prepared, was reduced at 250 °C for 2 h under a flow of hydrogen (30 ml/min).

Pluronic F127 block-copolymer (7.4 g) was dissolved in 384.3 g of 2 M HCl solution at 40 °C while stirring for 2 h. To it, 28.34 g of TEOS was added drop-wise over 30 min. The stirring was continued for 24 h. The gel formed was transferred into a Teflon-lined stainless steel autoclave (80 ml). It was crystallised at 80 °C for 48 h. The solid (as-synthesized SBA-16) formed was filtered out, washed with distilled water (2–3 l), dried at 100 °C overnight and calcined at 550 °C (heating rate = 4 °C/min) for 8 h. The calcined SBA-16 [27,28] was white in color. Yield: 96%. Pd was impregnated on SBA-16 as per the procedure reported above for Pd/SBA-12 wherein, SBA-16 instead of SBA-12 was taken.

2.2. Characterization techniques

X-ray powder diffraction (XRD) patterns were recorded on a X'Pert Pro Philips diffractometer equipped with Cu Kα radiation and a proportional counter detector. The measurements in the wide-angle region (2θ = 10–85°) were made at a scan rate of 4°/min and in the small-angle region (2θ = 0.5–5°) at 1°/min. High resolution transmission electron microscopic (HRTEM) images of the catalysts were recorded on a FEI Technai-F30 instrument fitted with a 300 kV field emission gun. Samples were prepared by dispersing the catalysts in *iso*-isopropanol, placing them on copper grids and drying the grids overnight at 25 °C. Specific surface area of the catalysts was determined from nitrogen adsorption-desorption isotherms recorded at −196 °C using a NOVA 1200 Quanta Chrome equipment. The BET method was adopted in estimation. The micropore volume was determined from the t-plot and average pore diameter was estimated following the Barret-Joyner-Halenda (BJH) model.

CO-chemisorption studies were conducted on a Quantachrome Autosorb iQ instrument. In typical experiment, about 0.2 g of the catalyst was taken in U-shaped quartz tube. It was first outgassed at 200 °C (heating rate = 20 °C/min) under a flow of He (20 ml/min) for 90 min and reduced with H_2 (20 ml/min) at 300 °C (heating rate = 20 °C/min) for 120 min followed by evacuating the sample at 300 °C for 120 min. Temperature of the sample was lowered down to 40 °C (in 1 min) under vacuum. CO was introduced and chemisorption measurements were started (equilibrium tolerance = 0, equilibrium time = 3 min, adsorption points = 80, 160, 240, 320, 400, 480 and 560 mmHg, analysis temperature = 40 °C, thermal equilibrium time = 10 min, leak test = 1 min). Specific surface area, percentage dispersion and average particle size of Pd were determined assuming the stoichiometric factor (S_f = number of moles of CO per surface Pd) as unity. In the average particle size determination, the particle shape factor (F) was considered as 6 assuming spherical or near spherical shaped particles. The following equations were used in determining the metal specific surface area (MS; m^2/g), percentage metal dispersion (D) and average metal particle size (d; in units of nanometers).

$$MS = \frac{V_m \times N_a}{S_f \times S_d \times L}$$

$$D = \frac{V_m \times AW \times 10^4}{\%W \times S_f}$$

$$d = \frac{F \times 10^3}{MS \times D_m}$$

Here, V_m is the CO-gas adsorbed at monolayer coverage (moles/g of catalyst), N_a is Avagadro number, S_d is metal surface density (i.e., number of metal atoms per square meter of Pd which is

0.127×10^{20}), AW is atomic weight of Pd (106.42), L is grams of Pd per gram of catalyst, %W is weight percent of Pd in the catalyst (which is equal to 100L) and D_m is density of Pd i.e., grams of Pd per unit volume (which is equal to 11.9 g/cm^3 at 20 °C).

2.3. Reaction procedure

Catalytic decarboxylation reactions are carried out in a stainless steel (Parr 300 ml) batch reactor equipped with a temperature controller. To quench the reaction immediately, the reactor vessel was fitted with an internal loop line cooler. Just prior to the reaction, catalyst was reduced at 250 °C (heating rate = 4 °C/min) for 2 h in a flow of hydrogen (20 ml/min). In a typical reaction, a known quantity of the substrate [oleic acid (OA), 99%; Loba Chemie; 2 g], solvent (decane, 99%; Spectrochem; 30 g) and reduced catalyst (10 wt% of the substrate) were taken in the reactor. The reactor was flushed thoroughly with hydrogen gas to remove the traces of air present in the vessel and then filled with hydrogen to a desired pressure (5–30 bar). The temperature of the reactor was raised to a desired value (300–325 °C) while heating at a rate of 4 °C/min and the reaction was conducted for 5 h. After the reaction, the rector was depressurized. The contents of the reactor were subjected to centrifugation. Catalyst particles were separated. Solvent was removed by rotary evaporator and the product was isolated. Deoxygenation reactions were conducted also with stearic acid (SA) and non-edible jatropha oil (JO). Fatty acid composition of jatropha oil is as follows: palmitic acid ($C_{16.0}$) = 15.6%, palmitoleic acid ($C_{16.1}$) = 1.0%, stearic acid ($C_{18.0}$) = 5.8%, oleic acid ($C_{18.1}$) = 40.1% and linoleic acid ($C_{18.2}$) = 37.6%.

2.4. Product analysis

For determination of acid values of reactants and products, 1 g of the sample was weighed and dissolved in a solvent mixture (10 ml) containing equal parts (v/v) of diethyl ether and ethanol; 3–5 drops of phenolphthalein indicator (1%, Merck, India) was added. Then, it was titrated with 0.1 N standardized sodium hydroxide solution until the color of the solution changed to light pink. Acid value of the sample was calculated using the formula:

$$\text{Acid Value} = \frac{V_{NaOH} \times N_{NaOH} \times 56.1}{W_{sample}}$$

here, 56.1 is the molecular weight of KOH as acid value is always reported as mg of KOH per g of sample. N_{NaOH} = normality of NaOH, V_{NaOH} = volume of NaOH consumed and W_{Sample} = weight of the sample taken for titration. Fatty acid (FA) conversion was determined from the acid values using the following formula:

$$\text{FA conversion (\%)} = \frac{(\text{Acid value of FA} - \text{Acid value of product sample})}{\text{Acid value of FA}} \times 100$$

In order to analyze by gas chromatographic (GC) technique, the product was derivatized with *N*,*O*-bis(trimethylsilyl) trifluoroacetamide (BSTFA). Known quantity of the product (0.015 g) was dissolved in pyridine (0.01 g) and 100 wt% excess of BSTFA was added to it. The mixture was then heated to 70 °C for 45 min and immediately injected in GC (Varian 450 GC; Select^{TM} Biodiesel column of dimensions: 15 m-length × 0.32 mm-diameter × 0.10 μm-film thickness). Helium was the cariar gas. In the GC method, injector and detector temperatures were set at 300 °C. A split ratio of 1:50 was used. The following temperature program was used: 80 °C (start) – 280 °C (at 20 °C/min ramp rate) – hold (10 min). Products were identified by GC–MS (Agilent Technology 7890 B; HP-5 column: 30 m-long, 0.25 mm-i.d.) and by comparing with standard samples. Products were analysed also by ^{1}H NMR (Bruker 200 MHz) and FTIR (Shimadzu) spectroscopies.

3. Results and discussion

3.1. Catalyst characterization

SBA-12 and Pd(1 wt%)/SBA-12 showed an intense peak at 1.68° arising from (002) and two weak peaks at 2.77° and 3.0° originating from (112) and (300) planes, respectively (Fig. 1). A weak shoulder appeared at 1.25° due to (100) reflection. These characteristics of SBA-12 were indexed to an ordered, three-dimensional, hexagonal mesoporous structure with a space group of $p6_3/mmc$ [27]. Except for some reduction in peak intensity, there was little change in the XRD peaks pattern and position after the deposition of Pd. In the wide-angle region, SBA-12 and Pd(1 wt%)/SBA-12 showed a broad peak at 22.2° arising from the amorphous silica in the pore wall structure. Two additional less intensity sharp peaks were observed at 40.2° and 46.6° for Pd(1 wt%)/SBA-12. These confirm the presence of metallic Pd, crystallised in a cubic closed-packed structure with a space group of $Fm\bar{3}m$ (JCPDS No. 05-0681). These reflections are originated from (111) and (200) planes of Pd^0, respectively. The above stated weak peaks in low and high angle regions were broad and diffused.

SBA-16 and Pd(1 wt%)/SBA-16 showed a strong peak at 0.9° attributable to (110) and weak peaks at 1.21° and 1.9° due to (200) and (211) reflections, respectively (Fig. 1). These distinct peaks of SBA-16 correspond to an ordered, three-dimensional, cubic, mesoporous structure with a space group of $Im\bar{3}m$ [28,29]. The chosen mesoporous silica supports (SBA-12 and SBA-16) differ in their pore structural arrangement. As is the case with SBA-12, metal deposition did not alter the framework structure of SBA-16. In the wide-angle region, Pd(1 wt%)/SBA-16 showed peaks due to metallic Pd at 40.3°, 46.9° and 68.6° arising from (111), (200) and (220) planes, respectively.

The presence of well-ordered mesopores in SBA-12 and SBA-16 materials was further confirmed by N_2-physisorption studies (Fig. 2). SBA-12 showed a type-IV adsorption isotherm with a hysteresis loop which could be assigned to H_1-type indicating ordered mesopores in the material. Adsorption isotherm of SBA-16 also showed a type-IV isotherm, however, with a H_2-type hysteresis loop confirming ordered mesoporous architecture. The H_2-type hysteresis loop indicates an ink bottle-neck shaped pores in the material [30]. No change in shape and hysteresis of the isotherms was observed after Pd deposition (Fig. 2). The physisorption isotherms of SBA-16 materials (Fig. 2) confirm the presence of cubic cage-like interconnected mesopore structure. All these materials showed narrow pore size distribution curves. Metal impregnation did not alter the shapes of hysteresis loops of SBA-12 and SBA-16. Textural properties of these catalysts are listed in Table 1. The SBA-12 materials had higher specific surface area (S_{BET}) than the SBA-16 materials. On loading Pd, the S_{BET} of SBA-12 increased from 708 to 804 m^2/g while it decreased from 574 to 489 m^2/g for SBA-16. Pore volume and average pore size remained nearly the same. This difference may be due to variation in Pd dispersion and metal-support contacts.

HRTEM images confirmed the long-range, three-dimensional, mesoporous ordering of these materials (Fig. 3). While Pd(1 wt%)/SBA-12 has hexagonally arranged pores, Pd(1 wt%)/SBA-16 has cubic, cage-like interconnected pore arrangement. Average particle size of Pd determined from the particle size distribution curve (Fig. 3) pointed out that the Pd particles on SBA-12 were larger in dimension (4.5 nm) than those on SBA-16 (2.5 nm). SBA-12 has higher specific surface area than SBA-16. One expects higher metal dispersion (lower particle size for Pd) on SBA-12 than

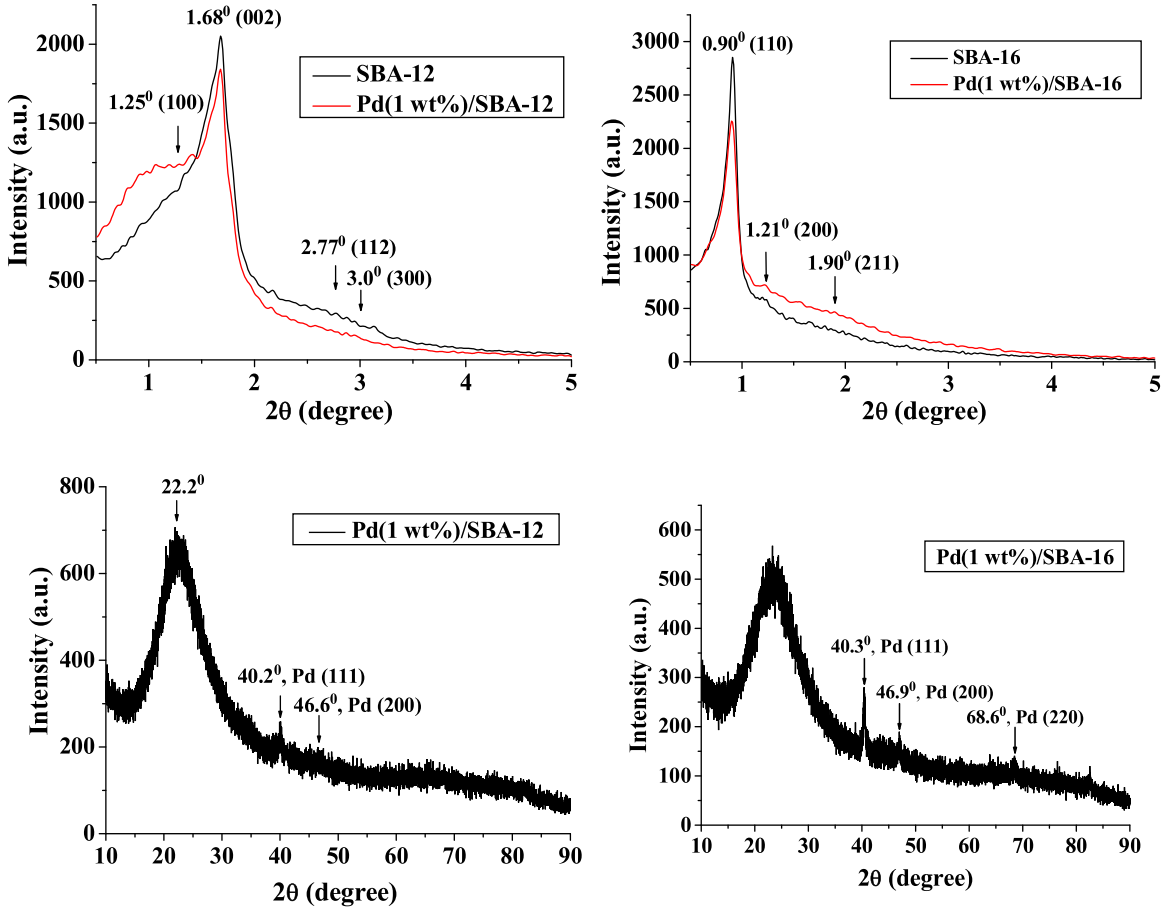

Fig. 1. XRD patterns of SBA-12, Pd(1 wt%)/SBA-12, SBA-16 and Pd(1 wt%)/SBA-16 in small- (top traces) and wide-angle (bottom traces) regions. Peaks due to different planes are marked.

Table 1
Textural properties of "bare" and Pd(1 wt%) supported on SBA-12 and SBA-16.

Catalyst	S_{BET} (m^2/g)[a]	Pore volume (cc/g)[b]	Average pore size (nm)[b]	Average Pd particle size (nm)[c]
SBA-12	708	1.0	2.3	–
Pd(1 wt%)/SBA-12	804	1.1	2.0	4.5
SBA-16	575	0.6	1.7	–
Pd(1 wt%)/SBA-16	489	0.6	1.7	2.5

[a] Calculated from N_2-physisorption (BET method).
[b] Calculated by BJH pore method.
[c] From HRTEM analysis.

on SBA-16. However, the reverse behavior points out the importance of surface structure (pore arrangement, hydrophobicity and acidity) on controlling the metal particle size.

CO-chemisorption studies revealed that surface area, metal dispersion and average particle size of Pd on SBA-12 and SBA-16 are nearly the same within the experimental error. Among the catalysts investigated, Pd(2 wt%)/SBA-16 had highest surface area and percentage metal dispersion and lowest Pd particle size (Table 2).

The surface hydrophobicity of SBA-12 and SBA-16 was quantified by thermogravimetric (TG) analysis. Calcined samples of SBA-12 and SBA-16 were exposed to water vapor at 25 °C and the amount of water adsorbed was analysed. Fig. 4 (left panel) shows the TG analysis of "bare" SBA-12 and SBA-16. SBA-16 showed water loss of 5 wt% below 127 °C. This was almost double for SBA-12 (10 wt%) [31]. The percentage loss of water normalised to surface area also followed the same trend (0.014 g/m^2 for SBA-12 and 0.009 g/m^2 for SBA-16). Thus, this experiment reveals that SBA-16 is relatively more hydrophobic than SBA-12. ^{29}Si cross-polarization magic-angle spinning nuclear magnetic resonance (^{29}Si MAS NMR) showed signals at around −91, −101, and −110 ppm attributed to three chemically and magnetically inequivalent tetra-coordinated Si species (Q^2, Q^3 and Q^4) having molecular formulae: $Si(OSi)_2(OH)_2$, $Si(OSi)_3(OH)$ and $Si(OSi)_4$, respectively [31]. SBA-12 showed a large amount of Q^2 and Q^3 species while SBA-16 had an excess of Q^4 species (Fig. 4 (right panel)). Higher amount of Q^4 species in case of SBA-16 materials is an indication of their surface hydrophobicity. This conclusion agrees with the observation made in water adsorption (TG) studies.

Total amount of acidic sites in SBA-12 and SBA-16 materials were quantified by temperature-programmed desorption of NH_3. These studies revealed that the supports were mildly acidic with the acid site density being 30 and 40 μmol/g for SBA-12 and SBA-16, respectively [31]. Thus the nature of the support has an influence on its surface structure and metal distribution.

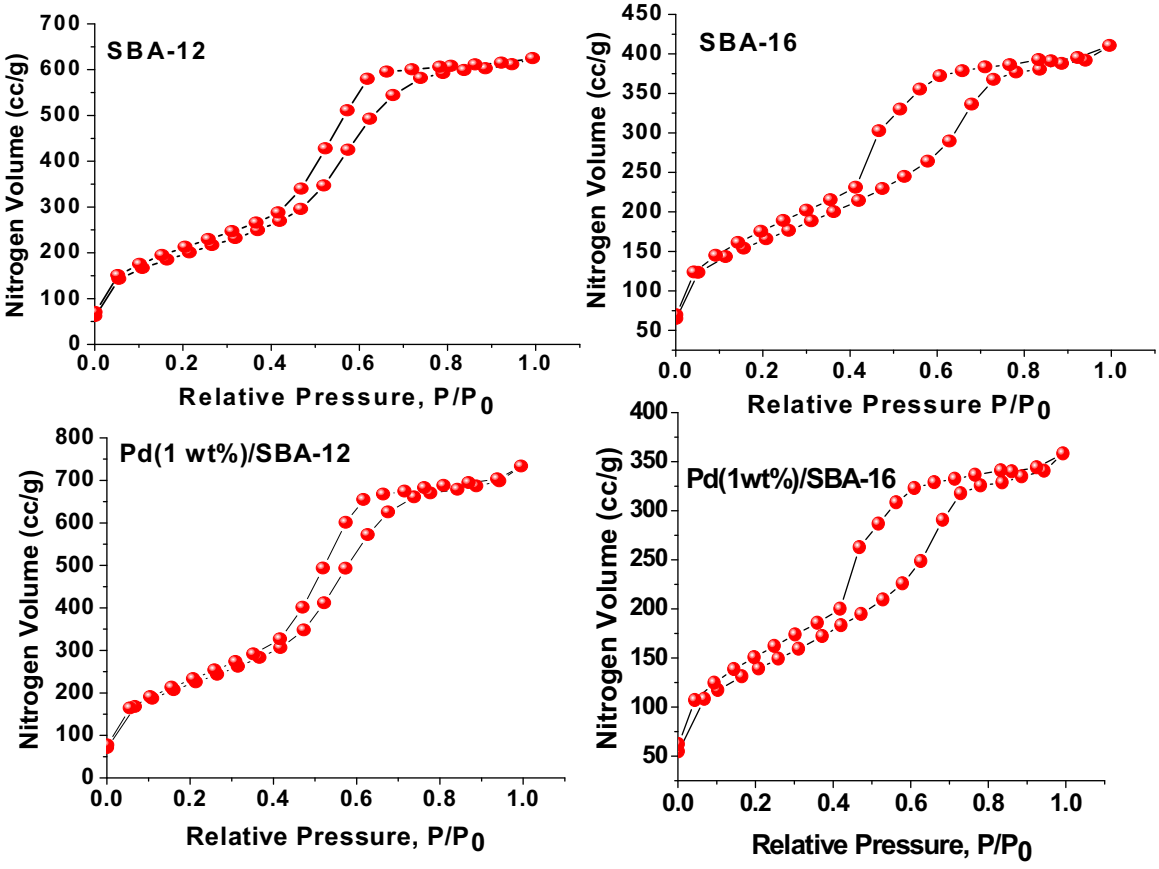

Fig. 2. Nitrogen adsorption-desorption isotherms of SBA-12, Pd(1 wt%)/SBA-12, SBA-16 and Pd(1 wt%)/SBA-16.

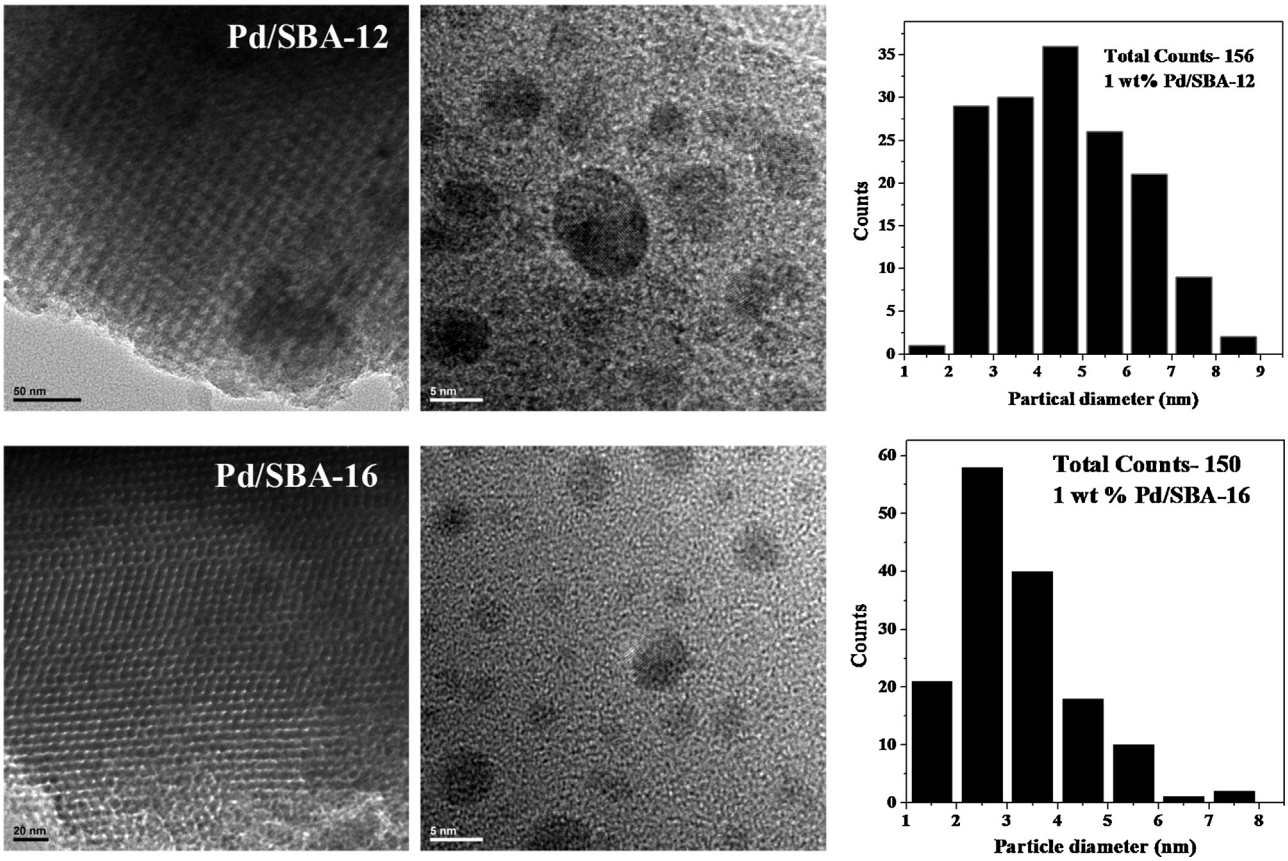

Fig. 3. HRTEM images and Pd particle size distribution of Pd(1 wt%)/SBA-12 and Pd(1 wt%)/SBA-16.

Table 2
CO-chemisorption data of supported Pd catalysts.

Catalyst	Monolayer uptake (μmol/g)	Active metal surface area (m^2/g of metal)	Metal dispersion (%)	Pd particle size (nm)
Pd(1 wt%)/SBA-12	10.13	48.0	10.8	10.1
Pd(1 wt%)/SBA-16	8.90	42.2	9.4	8.9
Pd(2 wt%)/SBA-16	27.68	65.6	14.7	27.7
Pd(3 wt%)/SBA-16	30.02	47.5	10.6	30.0
Pd(5 wt%)/SBA-16	43.52	41.3	9.2	43.5

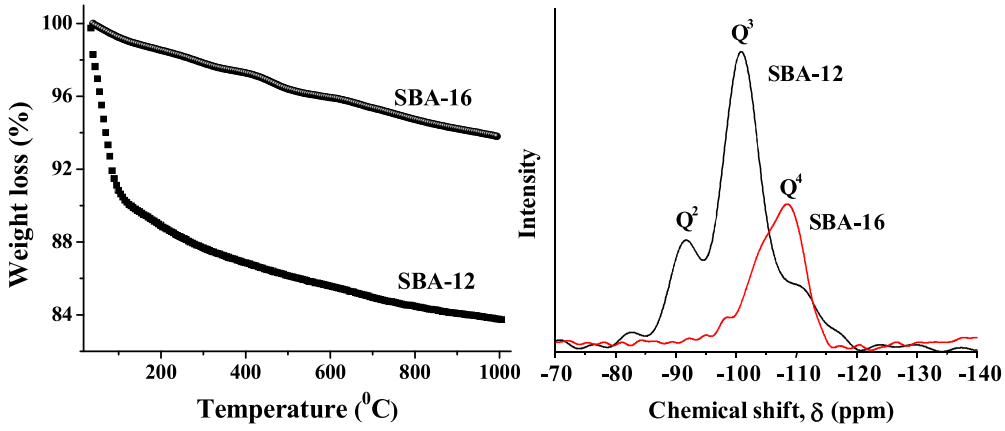

Fig. 4. Thermogravimetric analysis (left) and ^{29}Si MAS NMR of SBA-12 and SBA-16.

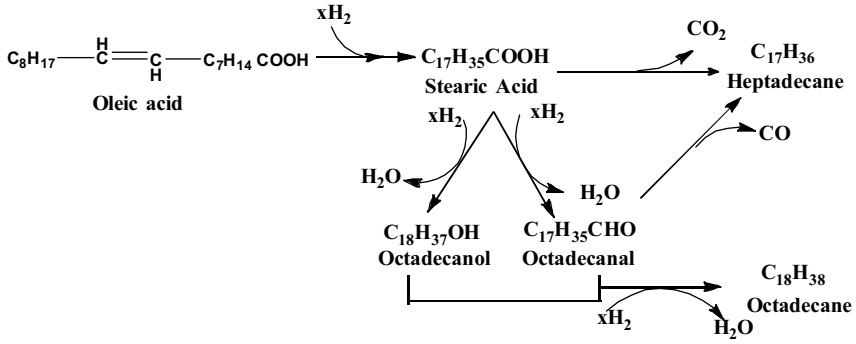

Scheme 1. Possible reaction pathway for deoxygenation of oleic acid.

3.2. Catalytic activity

Scheme 1 provides possible pathways for deoxygenation of FA. Oleic acid (OA), a representative FA, has two functional groups (C=C and COOH) for reaction with hydrogen. Hydrogenation of C=C (resulting in stearic acid, SA) happens prior to the deoxygenation reaction. Decarboxylation results in heptadecane (C_{17}) and hydrodeoxygenation yields octadecane (C_{18}). Octadecanol and octadecanal are the intermediates in the deoxygenation process. In reactions over Pd supported on SBA-12 and SBA-16, hydrocarbons (C_{17} and to a small extent C_{18}) are the major products and alcohols and aldehydes (others) are formed in small amount. Commercial grade OA and SA contained a small amount of palmitic acid (PA) impurity and hence, the deoxygenated product had some portion of C_{15} and C_{16} alkanes.

Temperature has a marked effect on the deoxygenation reaction. OA conversion (Fig. 5) and turnover frequency (TOF = moles of OA converted per mole of surface exposed Pd per hour; Table 3) increased linearly with temperature. Pd(1 wt%)/SBA-16 exhibited higher catalytic activity (OA converison and TOF) than

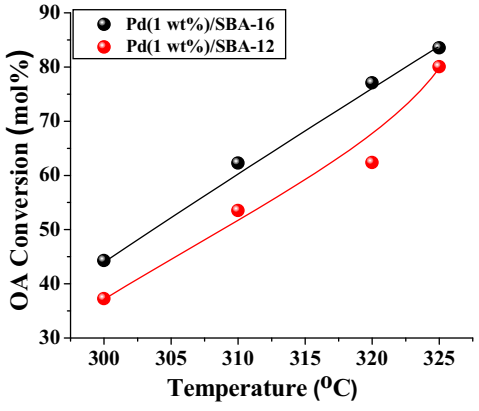

Fig. 5. Catalytic deoxygenation activity of Pd(1 wt%)/SBA-12 and Pd(1 wt%)/SBA-16. Reaction conditions: Oleic acid (OA) = 2 g, *n*-decane (solvent) = 30 g, catalyst = 0.2 g, H_2 pressure = 10 bar, reaction time = 5 h.

Table 3
Kinetic parameters in decarboxylation of oleic acid over Pd(1 wt%)/SBA-12 and Pd(1 wt%)/SBA-16[a].

Temperature (°C)	OA Conv. (mol%)	TOF (h^{-1})	$k \times 10^2$ ($L\,s^{-1}\,mol_{Pd}{}^{-1}$)	E_a (kJ/mol)
Pd (1 wt%)/SBA-12				
300	37.2	260	5.9	130.1
310	53.5	373	9.8	
320	62.3	435	12.5	
325	80.0	559	20.6	
Pd (1 wt%)/SBA-16				
300	44.3	352	7.5	127.1
310	62.3	495	12.4	
320	77.1	613	18.8	
325	83.5	664	23.0	

[a] Reaction conditions: Oleic acid (OA) = 2 g, *n*-decane = 30 g, catalyst = 0.2 g, p_{H2} = 10 bar, reaction time = 5 h.

Pd(1 wt%)/SBA-12. At 300 °C, the difference in OA conversion for Pd(1 wt%) supported on SBA-16 and SBA-12 was 7 mol%. Single point rate constants at different temperatures for both the catalysts were calculated using the following formula and assuming a pseudo-first order reaction,

$$k = \frac{-V \times \ln(1-X)}{W \times t}$$

where, k is the pseudo-first order rate constant ($L\,s^{-1}\,mol_{Pd}{}^{-1}$), X is OA conversion (in moles), V is volume of the reaction mixture (in litres), t is reaction time (in sec) and W is moles of Pd in the catalyst taken for reaction. Table 3 lists OA conversion, TOF and reaction rate constant at different temperatures (T) for the supported Pd(1 wt%) catalysts. The Arrhenius equation (given below) was employed to estimate the activation energy (E_a) and pre-exponential factor (A) for the decarboxylation reaction.

$$\ln k = \frac{E_a}{RT} + \ln A$$

Here, R is the gas constant (8.31 J/K mol) and T is the reaction temperature in Kelvin. From the plot of ln k versus 1/T, the values of E_a and A were determined. E_a was found to be 130.1 and 127.1 kJ/mol for Pd(1 wt%)/SBA-12 and Pd(1 wt%)/SBA-16, respectively. The value of normalised pre-exponential factor (A) for Pd(1 wt%)/SBA-12 and Pd(1 wt%)/SBA-16 was found to be 4.36×10^{10} and $2.98 \times 10^{10}\ s^{-1}$, respectively. As noted from the characterization studies SBA-16 is relatively more hydrophobic than SBA-12 and hence, adsorption of OA (hydrophobic molecule) is expected to be higher on the former than on the latter. Further, the average particle size of Pd on SBA-16 is lower (2.5 nm) than on SBA-12 (4.5 nm; HRTEM). Thus the exposed Pd atoms are higher in the case of the former than in latter. Both these factor (surface hydrophobicity and smaller Pd particles) are responsible for the higher catalytic activity of Pd(1 wt%)/SBA-16 than Pd(1 wt%)/SBA-12. Control experiments revealed that this reaction doesn't occur to a significant extent (under similar conditions) in the absence of a catalyst (OA conversion without catalyst was 2.4 mol% only). Also SBA-12 and SBA-16 supports do not catalyze the deoxygenation reaction. Popov and Kumar [32] estimated activation energy of 120 ± 5 kJ/mol for hydrothermal deoxygenation of OA over activated carbon (AC) in a continuous flow process. Fu et al. [33] reported E_a of 79 and 125 kJ/mol for hydrothermal decarboxylation of palmitic acid (PA) over AC-1 and 5% Pt/C catalysts, respectively. Snåre et al. [34] studied the decarboxylation of ethyl stearate over a Pd/C catalyst in semi-batch reactor and found E_a equals to 57.3 kJ/mol. While producing aviation fuel through decarboxylation of fatty acids in microalgae oil, Yang et al. [35] determined a value of 114 kJ/mol for the activation energy. The E_a values for the decarboxylation of OA over Pd(1 wt%)/SBA-12 and Pd(1 wt%)/SBA-16 catalysts fall within the range reported for the known catalyst systems. Catalytic activity of the present catalysts is comparable to that of Pd/SBA-15 [25,26].

At equal conversion of OA (62.3 mol%), the selectivity of Pd(1 wt%)/SBA-12 and Pd(1 wt%)/SBA-16 towards C_{17} (92.7 and 93.9%, respectively) and C_{15} (3.0 and 4.7%, respectively) HC products was nearly the same. This points out that particle size of Pd has little effect on the product selectivity. Temperature also had a negligible effect on C_{17} selectivity over Pd(1 wt%)/SBA-12 and Pd(1 wt%)/SBA-16 catalysts.

Table 4 presents the influence of hydrogen pressure and metal content on decarboxylation of OA over Pd/SBA-16 at 325 °C. OA conversion versus hydrogen pressure showed a parabolic type variation (Fig. 6). OA conversion increased with increasing hydrogen pressure up to 10 bar and then onwards showed a decreasing trend. Selectivity towards the hydrodeoxygenation (HDO) products (C_{18} and C_{16}) showed increasing trend with H_2 pressure. The selectivity for C_{17} decreased from 94.2% at 5 bar H_2 to 89.8% at 30 bar H_2. The possible reason for the decrease in conversion of OA at very high H_2 pressure (>10 bar) is the competition between hydrogen and OA for adsorption on the active site. Water is the byproduct in HDO process which could be a detrimental parameter for catalytic activity. An optimum pressure of 10 bar H_2 is ideal in terms of conversion and selectivity of the catalyst for the decarboxylation of OA to diesel range hydrocarbons. Decarboxylation took place at our reaction conditions even in the absence of external supply of hydrogen. OA conversion of 18.6% and C_{17} selectivity of 65.2 mol% were detected (Table 4). However, presence of hydrogen facilitated OA conversion and C_{17} selectivity.

Pd loading on SBA-16 has a positive effect on OA conversion. OA conversion increased from 83.5 mol% (at 1 wt% Pd loading) to 99.8 mol% (at 3 wt% Pd loading). Further increase in Pd loading (to 5 wt%) has no positive effect on OA conversion (Table 4). Pd loading has no major influence on the selectivity of the reaction.

Internal mass transfer is responsible for transport of reactant from entrance of catalyst pore pellet into the pore of catalyst pellet. If the concentration of reactant inside the pellet pore is lower than at the entrance of catalyst pore then reaction is limited by internal mass transfer. The effect of internal mass transfer was determined using Weisz-Prater criterion. According to this, the overall reaction kinetics is free from internal mass transfer limitation if the dimensionless Weisz number (Φ_I) is lower than 1, otherwise there would be influence of internal mass transport on the overall reaction kinetics [36,37].

$$\phi_I = \frac{r_{obs}\rho_p R_p^2}{D_{EA}C_{AS}}$$

In the above equation, r_{obs} is the observed higher reaction rate (1.1099×10^{-6} kg/kg s), ρ_p is the density of the catalyst pellet (1200 kg/m^3), R_p is the radius of catalyst particle (1 μm),

Table 4
Decarboxylation of oleic acid (OA) over Pd(1 wt%)/SBA-16: Influence of reaction parameters.

Effect of reaction temperature[a]							
Reaction temperature (°C)	OA conversion (mol%)[a]	TOF	Product selectivity (%)[b]				
			C_{18}	C_{17}	C_{16}	C_{15}	Others
300	44.3	352	1.2	94.4	0.2	3.5	0.7
310	62.3	495	0.5	93.9	0.2	4.7	0.6
320	77.1	613	1.0	93.5	0.2	4.5	0.8
325	83.5	664	1.1	93.3	0.1	4.7	0.7
Effect of H_2 pressure[b]							
H_2 pressure (bar)	OA conversion (mol%)[b]	TOF	C_{18}	C_{17}	C_{16}	C_{15}	Others
0	18.6	150	0	65.2	0	0.1	34.7
5	54.7	435	0.5	94.2	0.1	4.2	1.0
10	83.5	664	1.1	93.3	0.1	4.7	0.7
20	81.0	644	3.4	91.1	0.3	4.4	0.8
30	75.8	603	4.3	89.8	0.3	4.6	1.1
Effect of Pd content in the catalyst[c]							
Pd content (wt%)	OA conversion (mol%)[c]	*TOF*	C_{18}	C_{17}	C_{16}	C_{15}	Others
0	2.4	–	0	40.8	0	0	59.3
1	83.5	664	1.1	93.3	0.1	4.7	0.7
2	86.3	221	1.2	92.9	0.1	4.9	0.8
3	99.8	235	0.8	94.0	0.1	4.4	0.7
5	99.6	162	1.3	93.8	0.1	4.1	0.7

[a] Reaction conditions: OA = 2 g, *n*-decane (solvent) = 30 g, catalyst = 0.2 g, H_2 pressure = 10 bar, reaction time = 5 h.
[b] Reaction conditions: OA = 2 g, *n*-decane = 30 g, catalyst = 0.2 g, reaction temperature = 325 °C, reaction time = 5 h.
[c] Reaction conditions: OA = 2 g, *n*-decane = 30 g, catalyst = 0.2 g, H_2 pressure = 10 bar, reaction temperature = 325 °c, reaction time = 5 h. Others include octadecanol and octadecanal.

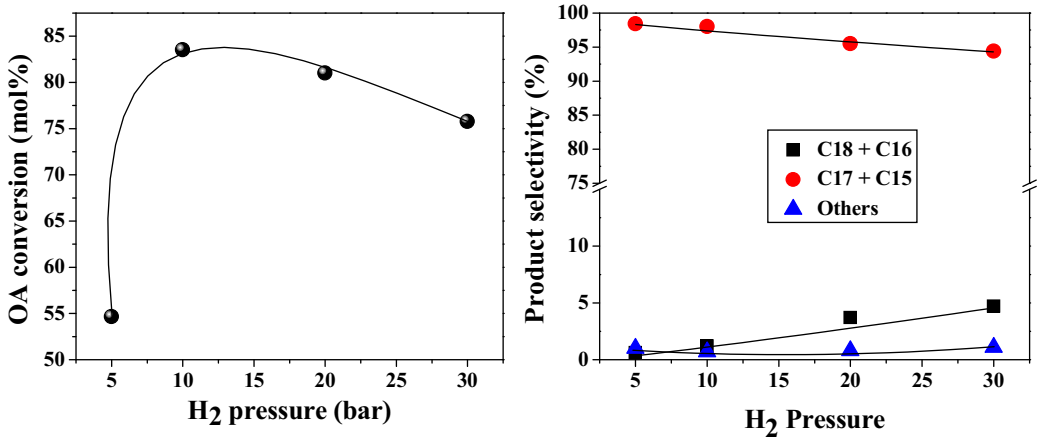

Fig. 6. Influence of hydrogen pressure on OA conversion and product selectivity. Reaction conditions: OA = 2 g, *n*-decane = 30 g, catalyst = 0.2 g, reaction temperature = 325 °C, reaction time = 5 h.

Table 5
Deoxygenation reaction over Pd(3 wt%)/SBA-16: Influence of feedstock.

Feedstock	Lipid conversion (mol%)	Product selectivity (%)				
		C_{18}	C_{17}	C_{16}	C_{15}	Others
OA	99.8	0.8	94.0	0.1	4.4	0.7
SA	92.3	13.7	80.2	0.9	4.2	1.0
JO	97.4	0.9	81.6	0.6	16.8	0.6

Reaction conditions: Fatty compound = 2 g, *n*-decane = 30 g, catalyst = 0.2 g, H_2 pressure = 10 bar, reaction temperature = 325 °C, reaction time = 5 h. Others include octadecanol and octadecanal. OA = oleic acid, SA = stearic acid and JO = jatropha oil.

D_{EA} is the molecular diffusion coefficient (1×10^{-10} m^2/s) [38] and C_{AS} is the concentration of reactant at catalyst surface (46.189 kg/m^3).

External mass transfer involves transport of hydrogen gas from bulk gas phase to external surface of the catalyst. This transport occurs through three main steps: (1) transport of hydrogen gas from bulk gas phase to solid-liquid interface, (2) diffusion of hydrogen gas into the liquid bulk phase consisting of OA and *n*-decane, and (3) transfer of dissolved hydrogen and OA onto the external surface of catalyst surface [39,40]. We have checked the possibility of external

mass transfer limitation using Mear's criterion. Accordingly to this criterion,

$$\phi_E = \frac{r_{obs} n \rho_p R_p}{k_S C_{AB}}.$$

Thiele modulus (ϕ_E) should be less than 0.15 for the reaction to be free from external mass transfer limitation. Here, n is the order of reaction (one in the present case), k_S is the external (liquid to solid) mass transfer coefficient (1.051×10^{-4} m/s) which can be calculated using the formula [41]:

$$N_{sh} = 2 + 0.36(N_{Re})^{3/4}(N_{Sc})^{1/3}$$

where, N_{sh} is the Sherwood number which is defined as $\frac{k_s d_p}{D_{EA}}$ wherein d_p is the particle diameter (2 μm), N_{Re} is the Reynolds number which is defined as $\bar{e}d_p{}^4/(\nu_L)^3$; $\bar{e}$ is the average specific power input per kg liquid (W/kg, assumed in the present case as 1) and ν_L is the kinematic viscosity of liquid phase (4.346×10^{-5} m^2/s), N_{Sc} is the Schmidt number which is defined as $\mu/\rho D_{EA}$; μ is the viscosity of liquid phase and ρ is density of liquid phase. C_{AS} is the surface concentration and C_{AB} is the bulk concentration of OA. It is assumed that $C_{AS} = C_{AB}$. From the above equations, we got $\Phi_E = 0.274 \times 10^{-6}$ and for $\Phi_I = 0.28 \times 10^{-6}$. As Φ_E and Φ_I are smaller than 0.15 and 1, respectively, there is no mass transfer limitation on reaction kinetics. Further, the SBA materials are mesoporous with pores in the range 1.7–2.0 nm (Table 1). The dimension of FA molecule is smaller than the pore size of SBA and hence, its internal transport should not be an issue. Except for the 1 wt% supported Pd which has a higher value, the TOF of 2–5 wt% Pd samples was nearly the same (Table 4) further confirming above conclusion related to absence of mass transfer limitation.

Pd(3 wt%)/SBA-16 was tested also for the deoxygenation of stearic acid (C_{18} saturated, SA) and non-edible jatropha oil (JA; triglyceride) at 325 °C for 5 h (Table 5). While near complete conversion of OA was observed, conversion of SA under similar conditions was somewhat lower (92.3 mol%). Hydrodeoxygenation (forming C_{18}) was more predominant with SA (selectivity = 13.7%) than with OA (0.8%). At the same time decarboxylation forming C_{17} was prevalent with OA (94%) than with SA (80.2%). In other words, the type of FA has certain effect on reactivity and reaction pathway. Based on the above results (differences in reactivity and product selectivity pattern with variation in the fatty acid type), it appears that SA is not the only intermediate to the final products formed from OA. At higher temperatures (300 °C and above), decarboxylation competes hydrogenation at the Pd site and the mechanism is all together different than reported in Scheme 1. A non-edible jatropha oil could be converted with significant efficiency (97.4 mol%) into C_{17} and C_{15} products. The catalyst showed high activity for each of these reactants portraying its efficiency in deoxygenation of structurally different feedstocks.

4. Conclusions

Palladium (1–5 wt%) supported on SBA-12 and SBA-16 catalyzed decarboxylation of FAs (OA and SA) and non-edible vegetable oil (jatropha) producing diesel-range hydrocarbons (C_{15}–C_{18}). Pd/SBA-16 showed higher catalytic performance than Pd/SBA-12 due to its higher surface hydrophobicity and metal dispersion. Nature of FA affected the reactivity and reaction pathway. At higher temperatures (300 °C and above), decarboxylation competes hydrogenation at the Pd site and hence, SA is not the only intermediate for the final products in OA decarboxylation reactions. Activity of these catalysts is comparable or higher than the hitherto reported catalysts for carboxylation of fatty acids.

Acknowledgement

This work forms a part of the Network project "Catalysts for Sustainable Energy (ECat; CSC 0117)."

References

[1] https://www.worldenergy.org/wp-content/uploads/2013/09/Complete_WER_2013_Survey.pdf.
[2] World Energy Outlook Special Report Energy and Climate Change, International Energy Agency, France (2015).
[3] B. Smith, C.G. Greenwell, A. Whiting, Energy Environ. Sci. 2 (2009) 262–271.
[4] P.M. Mortensen, J.-D. Grunwaldt, P.A. Jensen, K.G. Knudsen, A.D. Jensen, Appl. Catal. A: Gen. 407 (2011) 1–19.
[5] J.K. Satyarthi, T. Chiranjeevi, G.D.T. Shastry, P.S. Viswanathan, PTQ Q2 (2013) 1–5.
[6] S. Lestari, P. Mäki-Arvela, I. Simakova, J. Beltramini, G.Q.M. Lu, D.Y. Murzin, Catal. Lett. 130 (2009) 48–51.
[7] T.V. Choudhary, C.B. Phillips, Appl. Catal. A: Gen. 397 (2011) 1–12.
[8] E. Santillan-Jimenez, M. Cooker, J. Chem. Technol. Biotechnol. 87 (2012) 1041–1050.
[9] T. Morgan, E. Santillan-Jimenez, A.E. Harman-Ware, Y. Ji, D. Grubb, M. Crocker, Chem. Eng. J. 189–190 (2012) 346–355.
[10] M. Snåre, I. Kubičková, P. Mäki-Arvela, K. Eränen, D.Y. Murzin, Fuel 87 (2008) 933–945.
[11] J.G. Immer, M.J. Kelly, H.H. Lamb, Appl. Catal. A: Gen. 375 (2010) 134–139.
[12] T. Morgan, D. Grubb, E. Santillan-Jimenez, M. Crocker, Topics Catal. 53 (2010) 820–829.
[13] T. Kalnes, T. Marker, D.R. Shonnard, Int. J. Chem. Reactor Eng. 5 (48A) (2007) 1–19.
[14] A. Guzman, J.E. Torres, L.P. Prada, M.L. Nunez, Catal. Today 156 (2010) 38–43.
[15] L. Boda, G. Onyestyák, H. Solt, F. Lónyi, J. Valyon, A. Thernesz, Appl. Catal. A: Gen. 374 (2010) 158–169.
[16] J.G. Immer, M.J. Kelly, H.H. Lamb, Appl. Catal. A: Gen. 375 (2010) 134–139.
[17] R.W. Gosselink, S.A.W. Hollak, S.-W. Chang, J. van Haveren, K.P. de Jong, J.H. Bitter, D.S. van Es, ChemSusChem 6 (2013) 1576–1594.
[18] L. Hermida, A.Z. Abdulla, A.R. Mohamed, Renew. Sus. Energy Rev. 42 (2015) 1223–1233.
[19] M. Snåre, I. Kubičková, P. Mäki-Arvela, K. Eränen, D.Y. Murzin, Ind. Eng. Chem. Res. 45 (2006) 5708–5715.
[20] P. Mäki-Arvela, K. Kubičková, M. Snåre, K. Eränen, D.Y. Murzin, Energy Fuels 21 (2007) 30–41.
[21] S. Lestari, P. Mäki-Arvela, H. Bernas, O. Simakova, R. Sjöholm, J. Beltramini, G.Q.M. Lu, J. Myllyoja, I. Simakova, D.Y. Murzin, Energy Fuels 23 (2009) 3842–3845.
[22] K. Marata, Y. Liu, M. Inaba, I. Takahara, Energy Fuels 24 (2010) 2404–2409.
[23] M. Ahmadi, A. Nambo, J.B. Jasinski, P. Ratnasamy, M.A. Carreon, Catal. Sci. Technol. 5 (2015) 380–388.
[24] E.W. Ping, J. Pierson, R. Wallace, J.T. Miller, T.F. Fuller, C.W. Jones, Appl. Catal. A: Gen. 396 (2011) 85–90.
[25] S. Lestari, P. Mäki-Arvela, K. Eränen, J. Beltramini, G.Q.M. Lu, D.Y. Murzin, Catal. Lett. 134 (2010) 250–257.
[26] S.-P. Lee, A. Ramli, Chem. Central J. 7 (2013) 149.
[27] D. Zhao, Q. Huo, J. Feng, B.F. Chmelka, G.D. Stucky, J. Am. Chem. Soc. 120 (1998) 6024–6036.
[28] C.F. Cheng, Y.C. Lin, H.H. Cheng, S.M. Liu, H.S. Sheu, Chem. Lett. 33 (2004) 262–263.
[29] Y. Sakamoto, M. Kaneda, O. Terasaki, D. Zhao, J. Kim, G.D. Stucky, H. Shin, R. Ryoo, Nature 408 (2000) 449–453.
[30] P.I. Ravikovitch, A.V. Neimark, Langmuir 18 (2002) 9830–9837.
[31] A. Kumar, D. Srinivas, J. Catal. 293 (2012) 126–140.
[32] S. Popov, S. Kumar, Energy Fuels 29 (2015) 3377–3384.
[33] J. Fu, F. Shi, L.T. Thompson Jr., X. Lu, P.E. Savage, ACS Catal. 1 (2011) 227–231.
[34] M. Snåre, I. Kubičková, P. Mäki-Arvela, K. Eränen, J. Wärnå, D.Y. Murzin, Chem. Eng. J. 134 (2007) 29–34.
[35] C. Yang, R. Nie, J. Fu, Z. Hou, X. Lu, Bioresour. Technol. 146 (2013) 569–573.
[36] J.A. Lopez-Ruiz, R.J. Davis, Green Chem. 16 (2014) 683–694.
[37] C.A. Ferretti, R.N. Olcese, C.R. Apesteguĩa, J.I. Di Cosimo, Ind. Eng. Chem. Res. 48 (2009) 10387–10394.
[38] K. Belkacemi, A. Boulmerka, J. Arul, S. Hamoudi, Topics Catal. 37 (2006) 113–120.
[39] L. Zhou, A. Lawal, Energy Fuels 29 (2015) 262–272.
[40] H.S. Fogler, Elements of Chemical Reaction Engineering, 4th ed., Prentice Hall International Series in Physical and Chemical Engineering Sciences, New Jersey, 2011.
[41] A.A.C.M. Beenackers, W.P.M. Van Swaaij, Chem. Eng. Sci. 48 (1993) 3109–3139.